COLOR LINE SCANNER AS IMAGING NDVI SENSOR[1]

A. BOCHERT, J. M. HACKER*, K. OHM

Alfred Wegener Institute for Polar and Marine Research,
Columbusstrasse, D-27568 Bremerhaven, Germany, tel: +49 471 4831 1172,
fax: +49 471 4831 149, e-mail: abochert@awi-bremerhaven.de

*Airborne Research Australia, Flinders University, GPO Box 2100, Adelaide 5001,
Australia, tel: +61 8 8182 4000, fax: +61 8 8285 6710, e-mail: jhacker@es.flinders.edu.au

KEY WORDS: airborne imager, vegetation, NDVI, high-resolution, low-cost, geo-coding

ABSTRACT

A new low-cost high-resolution line scanner has been developed at the Alfred Wegener Institut for Polar and Marine Research in Germany. For NDVI applications the Color Line Scanner (CLS) measures the solar radiation reflected by the ground surface in the spectral ranges of 500nm to 570nm (green), 580nm to 680nm (red) and 720nm to 830nm (near infrared). With the red and near infrared spectral bands the NDVI can be calculated in order to map vegetation. The line scanner supports a resolution of 2048 pixels per line for each spectral band. During data acquisition 50 lines per second are stored yielding a maximum spatial resolution of better than 0.5m. With DGPS and attitude measurements (INS or Vector GPS) it is possible to geo-reference the line scanner data into a map format with an absolute accuracy of a few metres. Several images can be combined to cover large areas. After the determination of mounting errors the geo-referencing into a map is carried out automatically without manual adjustments. The CLS was first used as an imaging NDVI sensor at Airborne Research Australia (ARA) the Major National Research Facility at the Flinders University of South Australia to investigate spatial and temporal variations of vegetation cover.

1 INTRODUCTION

Various airborne line scanner systems have been developed at the Alfred Wegener Institute for the visible, near infrared and thermal infrared spectral ranges. These line scanners are mainly used for the purpose of validating satellite data (Bochert 1996 and 1999). For other applications the area surveyed is being imaged with the aim to investigate the interaction between meteorological processes and the Earth's surface (Kottmeier *et al.* 1994 and Hartmann *et al.* 1996). The Color Line Scanner (CLS) can be used as an imaging NDVI (Normalized Difference Vegetation Index) sensor to map surface vegetation over large areas.

With DGPS and aircraft attitude measurements (pitch and roll angles and heading derived from INS or Vector GPS) it is possible to geo-reference the line scanner data into a map format with an absolute accuracy of a few metres. In this way several images can be combined to cover large areas. After the determination of mounting errors the geo-referencing into a map is carried out automatically without manual adjustments or sophisticated correlation algorithms. The post-processing software of the CLS

[1]Second EARSeL Workshop on Imaging Spectroscopy, Enschede, 11–13 July 2000

enables a short turn around time. Geo-referenced NDVI maps are available a few hours after the measuring flight.

The whole development was focused on cost efficiency and light weight. The sensor itself, a 2048 colour linear CCD was available on the commercial marked as mass-produced article. The optical system is based on lenses of 35mm cameras. Dedicated software for acqusition and post-processing is used for the system operation. Data acqusition with a personal computer on a hard disk is a fast and simple method. The possibility of the operation from a motor glider results in very low operational costs.

2 THE COLOR LINE SCANNER

The CLS was developed at the the Alfred Wegener Institute in cooperation with the Hochschule Bremen in Germany. The development is based on a Charge Coupled Device (CCD) linear sensor designed for colour photocopiers and scanners. This leads to the posibility of cost effective multispectral imagery with a single camera system.

The CLS is a cross-track scanner which measures the intensity of surface signals scanned perpendicularly to the flight track. The image lines are recorded with a swath angle of up to 90 degrees and consist of 2048 pixels. The altitude of the aircraft determines the width and cross-track resolution of the images. Since the scanner allows a sampling of 50 lines per second, the along-track resolution is determined by the ground speed of the aircraft. With a typical speed of 50m/s the along-track resolution is one metre. The image lines are digitized during the measurement and stored on a hard disk of a personal computer. With a resolution of one metre on the Earth's surface a 10 GByte hard disk stores the image data of around 3000km^2.

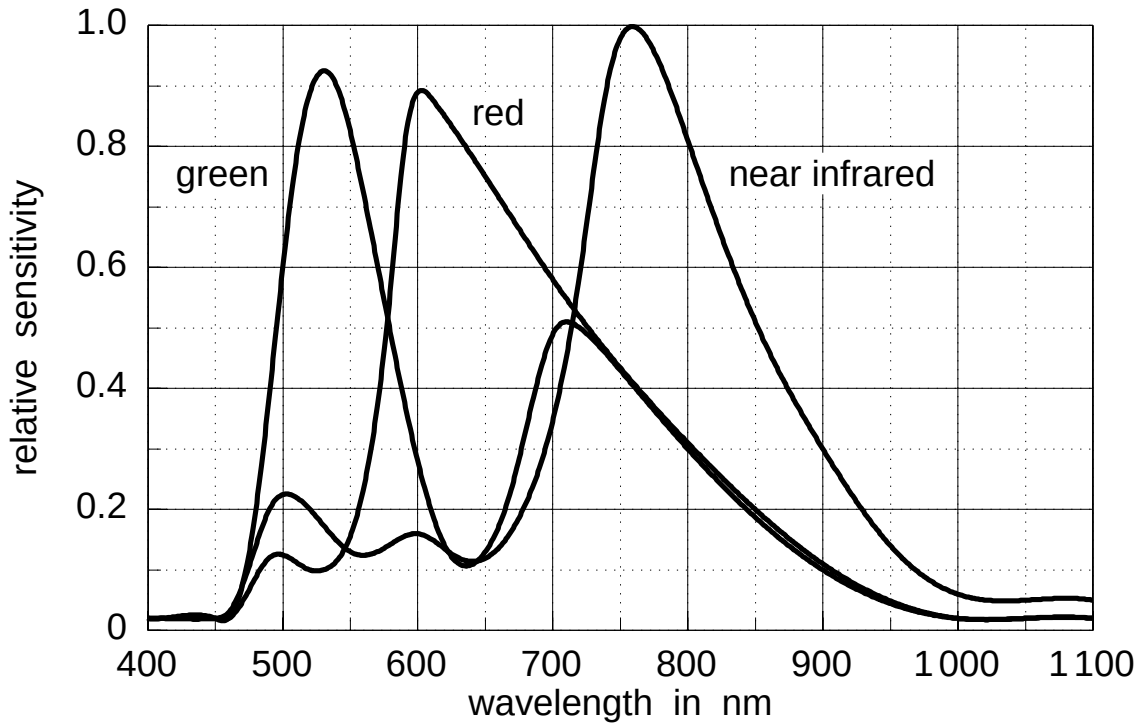

Figure 1: Relative sensitivity of the Color Line Scanner used as NDVI sensor.

For NDVI applications the CLS measures the solar radiation reflected by the ground surface in the spectral ranges of 500nm to 570nm, 580nm to 680nm and 720nm to 830nm. With the red and near infrared spectral band the NDVI can be calculated in order to map vegetation. Figure 1 shows the relative sensitivity of the CLS used as NDVI sensor. For other applications the near infrared band can be changed to a blue band yielding an RGB image. The resolution of 2048 pixels per line is supported for each spectral band. A CCD linear image sensor is used as a detector. Since each sensor element for all spectral bands is included in a single line the synchronization of the three spectral bands is simple. Each color pixel consists of three sensor elements of the size of 7μm $\times$ 21μm with 7μm pitch to form a 21μm $\times$ 21μm pixel with 21μm pitch. The lenght of the linear sensor array of 43mm enables the use of common lenses of 35mm cameras, thus an easy adjustment of the swath angle with the change to different focal lengths.

In addition to the 6144 spectral sensor elements, optically black sensor elements are available to measure the dark current of the CCD. Corrections for dark current and other known characteristics of the individual sensor elements are applied during post-processing of the image data. The calibration of the CLS is necessary for the calculation of the NDVI. During data acquisition the pixel intensities are converted into a byte value for each spectral band.

The acquisition of an image line can either be controlled by an internal timer or by means of an external trigger pulse. The external pulse can be used to synchronize the scanner to other data streams, such as the GPS and aircraft attitude data.

The line scanner was flown on several aircraft. In the Dornier DO228 polar research aircraft of the Alfred Wegener Institute the scanner unit is mounted above a roller door in the cabine floor, in the ARA Cessna 404 Titan, it is fitted into a pod underneath the fuselage. In both cases the scanner unit is protected from dust and stones during take-off and landing. The use of the ARA Grob G109B motorglider results in a very high spatial resolution of 0.4 metres on the ground and low operational costs. Due to the small size of the scanner (110mm$\times$110mm$\times$300mm) it is mounted in a leading edge pod on a wing.

3 NORMALIZED DIFFERENCE VEGETATION INDEX

Each object on the Earth's surface reflects electromagnetic radiation of various wavelengths in its own characteristic way. This fingerprint allows recognition and separation of objects. The spectral characteristics of vegetation and soil are of special interest for this work. This investigation will concentrate on the reflectance in the visible and near infrared wavelength.

The spectral reflectance of an individual leaf is caused by the leaf pigments and the cell structure (Eiden *et al.* 1991). Mainly the leaf pigments chlorophyll and carotene determine the reflectance properties in the visible wavelengths from 400nm to 700nm. For this range figure 2 shows that leaves have their maximum absorption in the blue and red spectral bands whereas green light is reflected more, which makes leaves appear green. In the near infrared, between 700nm and 1300nm, the reflectance of green leaves reaches a broad maximum. This high reflectance in the near infrared band is caused by the internal cell structure of the leaves. The steep increase of reflectance with a maximum slope around 690nm to 740nm is a typical phenomenon of vegetation. It is called the red edge. Pinar and Curran (1995) outlined that the content of chlorophyll is strongly correlated to the position of the red edge. An increase in chlorophyll concentration causes a broadening of the chlorophyll absorption feature and this will move the long wavelength boundary of the chlorophyll absorption feature and thereby the red edge to longer wavelengths.

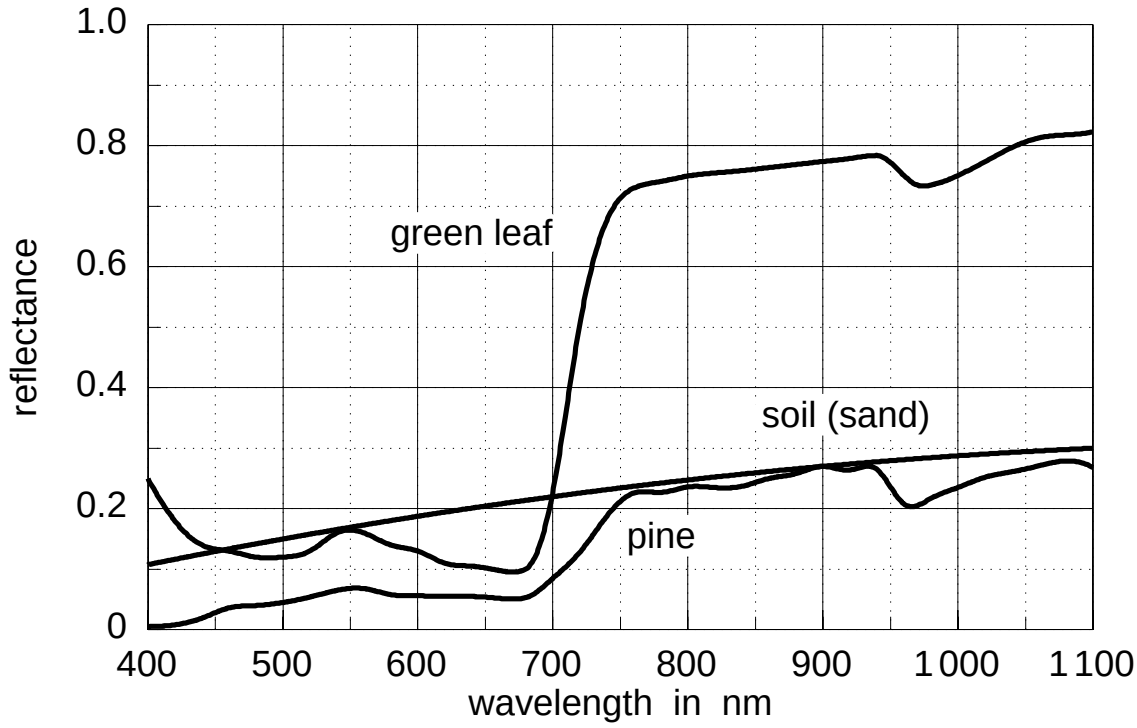

Figure 2: Spectral reflectance of green leaves (Eucalyptus) (Datt 1998), pine (Dawson *et al.* 1998) and bare soil (sand) (Eiden *et al.* 1991).

The spectral reflectance of soil is determined extensively by the character of the soil surface. In general, soil reflectance increases steadily with wavelength (figure 2). The reflectance is mainly dependent on the concentration of moisture, organic matter and iron oxide. As the moisture content of the soil increases the reflectance in the spectral range from 400nm to 1300nm decreases continously. The water absorption bands are at longer wavelengths. Organic matter decreases the reflectance, particularly in the range above 600nm. According to Eiden *et al.* (1991) with increasing iron oxide content, the reflectance of soil decreases significantly in the green range and increases in the red spectral range. Apart from mineral composition, the mineral grain size is of great importance. The reflectance rises continuously as grain size falls.

For remote sensing the transition from small to large scale observations, thus from single type surfaces to a mixture of different surface types has to be carried out. For a measured area which is only partially covered by vegetation the total reflectance consists of a combination of both vegetation and soil. The total reflectance of the mixed area can be calculated by Kirchhoff's law according to the proportional coverage by each surface type. According to the investigations of Wardley (1984) the relative spectral dependencies of the reflectance of natural materials could be approximated for the visible and near infrared spectral ranges as a Lambert reflectance. In a simple case of a flat terrain, with the known spectral characteristics of the surface types we can calculate the percentage of each type from the measured spectrum. This calculation is not dependent on the angle of measurement, thus not a function of the pixel location with line scanner measurements. Due to the restrictions to relative spectral dependencies, the work of Wardley (1984) shows that such measurements with large variations of viewing angles like airborne line scanner measurements can only use ratioed vegetation indices like the NDVI rather than non-ratioed indices.

Difficulties arise if we take the shape of, for example the vegetation, into account. Figure 3 illustrates that in case of a forest a nadir angle of measurement enables a contribution of the soil. With rising angles the signal increasingly comes from the treetops. Since the line scanner measures reflected radiation rather than reflectance the corresponding problem arises with the shadowing of the soil.

Mainly the soil will be covered by vegetation which lowers the contribution of the soil. In the presented work no measures were taken against this angle dependence.

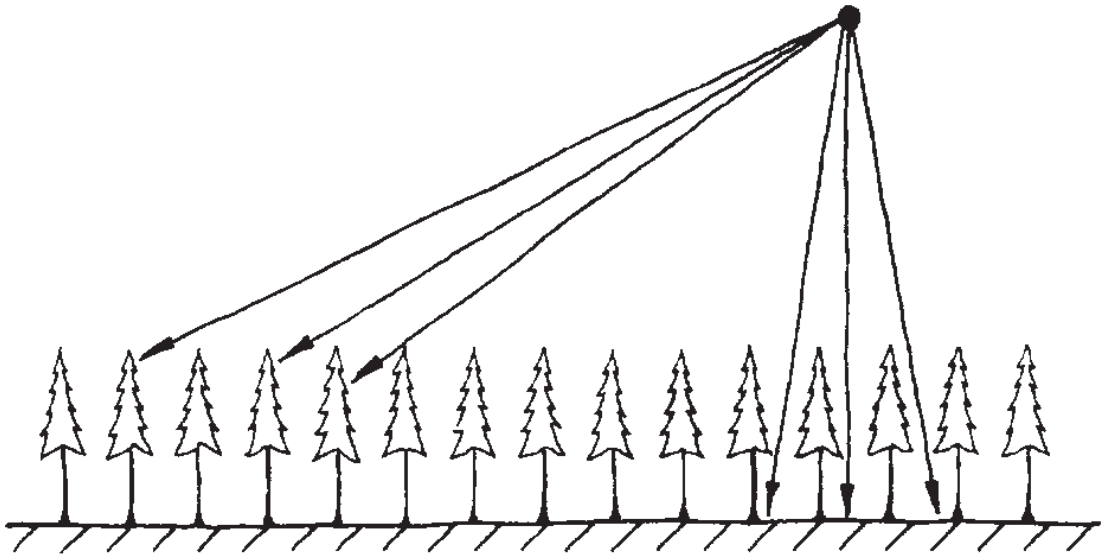

Figure 3: Importance of the angle of measurement and the relevant surfaces (Bochert 1992).

Large scale observations are connected to the measurement from a remote distance. With further distance the influence of the atmosphere has to be taken into account. According to Eiden *et al.* (1991) the main problem is caused by clouds and even optically thin clouds. There are only insignificant water vapour absorption bands in the spectral range from 400nm to 1100nm (Justice *et al.* 1991). Using airborne remote sensing the distance through the atmosphere is short in comparison with satellite remote sensing, thus the influence of the atmosphere is negligible. Only clouds between the surface and the aircraft have to be taken into account during the measurement.

Frequent and varying cloud cover is a major logistical problem for optical remote sensing studies in polar regions. Although McMichael *et al.* (1999) used ground based measurements, cloud cover results in shadow problems on the Earth's surface. They have investigated the impact of varying illumination conditions on spectral measurements in the red and near infrared spectral range. They came to the result that the NDVI as a ratioed vegetation index is not affected by illumination variations derived by cloud shadows. With their further work (Hope et al. 1999) they restrict this statement to thin cloud cover since the absorption and scattering of solar radiation by cloud droplets and water vapor is greater in the near infrared wavelength than in the visible part of the spectrum. Since the relations of the absorption in both spectral bands are strongly linear to the optical thickness of the cloud cover NDVI measurements can be corrected for thick cloud cover.

Numerous vegetation indices have been developed to characterize vegetation canopies. Eiden *et al.* (1991) have investigated the NDVI, the Perpendicular Vegetation Index (PVI), the Soil Adjusted Vegetation Index (SAVI), and the Transformed Soil Adjusted Vegetation Index (TSAVI). All these vegetation indices have the use of the red and near infrared bands in common. The Perpendicular Vegetation Index and the Transformed Soil Adjusted Vegetation Index requires further background of the specific soil which has to be changed with the location of measurement, is thus difficult to find. Eiden *et al.* (1991) came to the result that the NDVI is easy to calculate and the other tested vegetation indices do not result in a remarkable improvement. The NDVI is commonly accepted as a standard approach for satellite based vegetation surveys. Thus, the results are comparable with other investigations.

The NDVI V_{NDVI} is calculated by the difference of the intensities of the reflected radiation in the near infrared and the red bands divided by their sum:

$$V_{NDVI} = \frac{I_{nir} - I_{red}}{I_{nir} + I_{red}} \tag{1}$$

I_{nir} is the intensity of the near infrared spectral band and I_{red} the intensity of the red band. The formation of the quotient eliminates the influence of variations in illumination which turns the investigation to a comparison of the reflectance.

With the transition to large scale observations where a single pixel covers different surface types the NDVI is mainly determined by vegetation density and greenness. Vegetation density is defined as the ratio of the vegetated area and the total area covered by a pixel. The greenness is defined as the NDVI of a pure vegetation pixel without soil and thus it reflects the health of the vegetation and its chlorophyll concentration. With this it shows the ability of photosynthesis. Analyzing equation (1) with the data of figure 2 but with soil of different reflected intensity it becomes obvious that the brightness of the soil becomes important. With a black soil the NDVI will not change with vegetation density. With a constant vegetation density a lighter soil will result into a lower NDVI, whether it is due to its reflectivity or the illumination of the soil. Returning to the example of figure 3 and a resolution which covers several trees, with a black soil the NDVI is not a function of the angle of measurement, whereas with a lighter soil it is. If we suppose a nadir looking measurement with a non black soil the NDVI will increase with the sun angle as long as the soil is shadowed, because the brightness of the soil will decrease in comparision to the trees. If the soil is not shadowed the NDVI will not change with the sun angle as it does for the higher angles of measurement.

Beyond the NDVI the leaf area index (LAI) is an often used parameter for ecological studies. To map LAI, the relationship between spectral data and ground measured LAI has been investigated by Leblance *et al.* (1999). They found an exponential relation between the NDVI and LAI with a saturation of NDVI higher than 0.86. The simple ratio of the near infrared and red spectral band shows a linear relation to LAI but is more scattered.

4 COMPARISON WITH OTHER NDVI SENSORS

Compared to the CLS, most of the established NDVI sensors use filters with much sharper edges on both the long and short wavelengths of the spectral bands. It is therefore important to evaluate possible effects due to this difference on the NDVI.

Figure 4 shows the spectral sensitivity of the CLS in comparison with those of some satellite-borne scanners as given by Kramer (1996). The red band of the CLS extends from 580nm to 680nm, and the near infrared from 720nm to 830nm. In comparison with the sensitivity of the National Oceanic and Atmospheric Administration's (NOAA) Advanced Very-High Resolution Radiometer (AVHRR) the spectral part of the longer wavelength in the near infrared band is missing. The other sensors have a slightly different sensitivity. These sensors are operated on the Landsat (MSS - Multi Spectral Scanner, and TM - Thematic Mapper) and SPOT (HRVIR - High Resolution Visible and Infrared Sensor, and VEGETATION) satellite.

The effect of the comparatively small slope of the CLS sensitivity for wavelengths shorter than 580nm and longer than 830nm can be assumed to be of little effect on the NDVI, because there are only insignificant water vapour absorption bands in the whole spectral range from 400nm to 1100nm (Justice *et al.* 1991).

Of greater importance is the overlap of the bands in the area around 700nm, because an increase of the near infrared radiance also contributes to the red band. This lowers the radiative contrast between vegetation and soil. In the following, a range of specific surface types is used to evaluate the influence of this overlap on the value of the NDVI in comparison with other NDVI sensors.

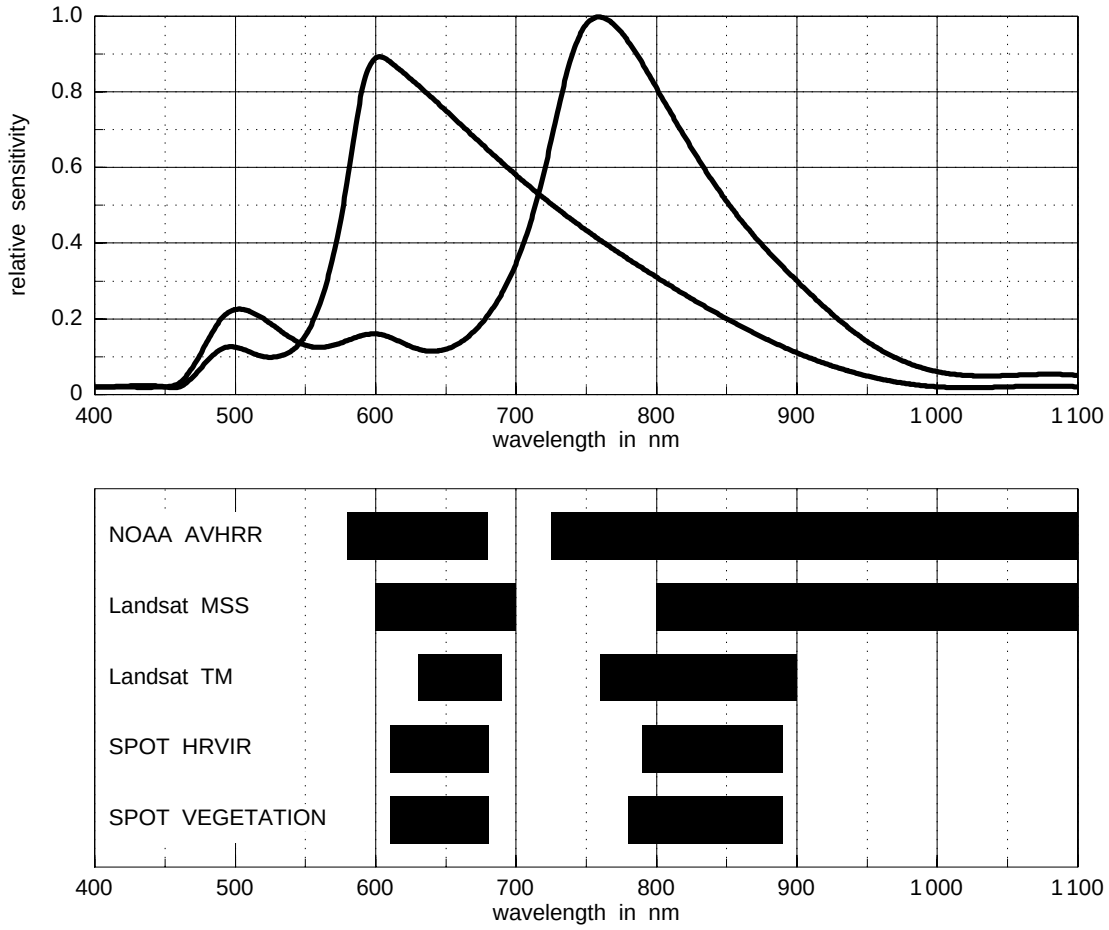

Figure 4: Relative sensitivity of the Color Line Scanner in comparison with satellite sensors (Kramer 1996).

Figure 5 shows the spectral reflectance of seven different surface types. The three types of leaves represent Eucalyptus (Datt 1998) with diffent concentration of chlorophyll. Pinar and Curran (1996) explained that an increase in chlorophyll concentration causes a broadening of the chlorophyll absorption feature. This will move the long wavelength boundary of the chlorophyll absorption feature and with this the red edge to longer wavelengths. This means that leaf 3 in figure 5 could be more active than the other two leaves. The spectral reflectance of pine is measured from a thick layer of needles (Dawson *et al.* 1998). The soil is an example of sand from Eiden *et al.* (1991). The reflectance of soil will change with a different type of material as well as with different moisture content. But the relative pattern will not change much. To simulate the measurement of the NDVI there are two mixed areas included. Mix 1 is an area with half soil and half leaves of type 2. Mix 2 contains two third of soil and only one third leaves of type 2. These are simulating mixed pixel measurements.

As mentioned above, the absolute value of the NDVI will be most affected by the overlap around 700nm in the CLS sensitivity curves. It is therefore desirable to derive a scaling factor which translates the CLS NDVI measurements to those from one of the most common sensors, the NOAA AVHRR. For areas completely covered with leafs of type 2 (figure 5), the AVHRR will measure an NDVI of $V_{NDVI\ AVHRR} = 0.75009$, whereas the CLS will measure an NDVI of $V^*_{NDVI\ CLS} = 0.27735$. A

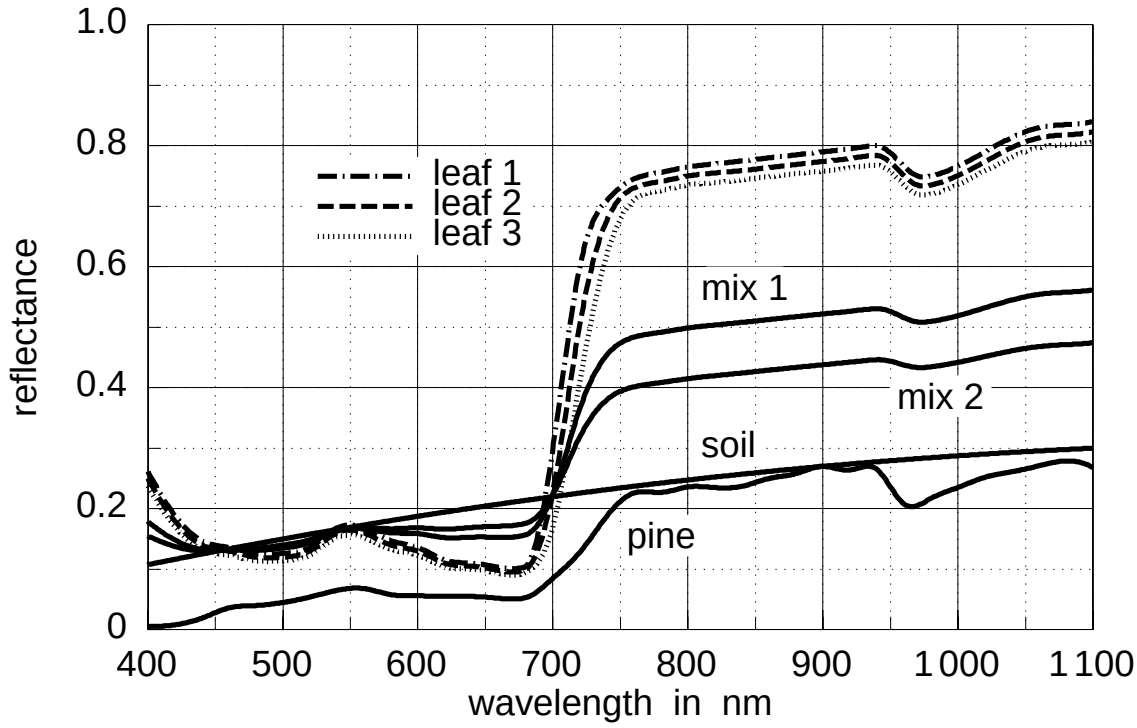

Figure 5: Spectral reflectance of green leaves (Eucalyptus) (Datt 1998), pine (Dawson *et al.* 1998), bare soil (sand) (Eiden *et al.* 1991) and mixed areas. Leaf 3 is between leaf 1 and leaf 2.

scaling factor S defined by

$$S = \frac{V_{NDVI\ AVHRR}}{V^*_{NDVI\ CLS}} = \frac{0.75009}{0.27735} = 2.7045 \tag{2}$$

can therefore be applied to correct the CLS NDVI measurements for the overlap. Assuming that the value of S can also be used for other surfaces, equation (1) can be extended for CLS NDVI measurements to

$$V_{NDVI} = S\ \frac{I_{nir} - I_{red}}{I_{nir} + I_{red}} \tag{3}$$

Using equation (3) for the CLS and equation (1) for all other sensors, the NDVI was computed for the different surface types as listed in figure 5. Sensors used in this comparisons were the Flinders Institute for Atmospheric and Marine Sciences' (FIAMS) VEG Meter (Bannehr 1990), the NOAA AVHRR and the LANDSAT TM. The VEG Meter of FIAMS is sensitive over narrow bands at 630nm and 830nm. Table 1 shows beside the simulated NDVI values the diffences to the NDVI drived from the CLS.

Since the CLS is adjusted to the AVHRR with leaves of type 2 there is no difference from the NDVI of the AVHRR. All the other simulations resulted in differences of up to $|\delta| = 0.031$ for the VEG Meter with pine. For leaf 2 the VEG Meter and the TM will result into a slightly higher NDVI with a difference of $|\delta| = 0.009$ and $|\delta| = 0.013$. But per definition the same difference applies to the NDVI of the AVHRR. The comparison between the three types of leaves is interesting. It was mentioned that leaf 3 contains more chlorophyll than the other two and with this it is more active. The overlap of the bands of the CLS enables the detection of the shift of the red edge where the other sensors have only small changes.

The highest difference of NDVI between the CLS and the satellite sonsors occur for bare soil;

	airborne and spaceborne NDVI sensors						
	CLS	VEG Meter		NOAA AVHRR		LANDSAT TM	
	V_{NDVI}	V_{NDVI}	δ	V_{NDVI}	δ	V_{NDVI}	δ
leaf 1	0.733	0.760	+0.027	0.752	+0.019	0.761	+0.028
leaf 2	0.750	0.759	+0.009	0.750	+0.000	0.763	+0.013
leaf 3	0.767	0.758	-0.009	0.748	-0.019	0.765	-0.002
pine	0.651	0.620	-0.031	0.634	-0.017	0.636	-0.015
soil	0.129	0.126	-0.003	0.154	+0.025	0.101	-0.028
mix 1	0.550	0.544	-0.006	0.546	-0.004	0.534	-0.016
mix 2	0.447	0.438	-0.009	0.446	-0.002	0.423	-0.024

Table 1: Comparison of the NDVI of the Color Line Scanner to different airborne and spaceborne NDVI sensors. The VEG Meter is flown on ARA aircraft (Bannehr 1990), it is sensitive at 10nm narrow bands around 630nm and 830nm. δ gives the difference to the Color Line Scanner.

$\delta = +0.025$ for AVHRR and $\delta = -0.028$ for TM. Nevertheless the different signs results in a difference of $|\delta| = 0.053$ (number not in table 1) between the NDVI of AVHRR and TM which is the highest difference for this simulation. For bare soil the NDVI of the VEG Meter is close to that of the CLS.

Comparisons could be used to assess the values of the differences δ in table 1 the mean differences of the absolut values $|\delta|$ for the sensor. To the AVHRR and TM these are $\overline{|\delta|} = 0.012$ and $\overline{|\delta|} = 0.018$, to the VEG Meter $\overline{|\delta|} = 0.013$ (numbers not in table 1). The comparison to the mean differences between the AVHRR and the TM $\overline{|\delta|} = 0.018$ leads to the result that the NDVI derived from measurements of the CLS is as reliable as the NDVI from the satellite sensors. These data could even be compared with each other.

5 RADIOMETRIC CORRECTIONS AND CALIBRATION

The radiometric correction concentrates on the differences of each single sensor in comparison to all other sensors. The calibration of the CLS ensures an equal response of the different spectral channels necessary for the calculation of the NDVI.

Beside 78 optically black sensor elements 6144 sensor elements of the CLS are used to measure the sun radiation reflected on the ground. Due to manufacturing variations these sensor elements have different dark currents and sensitivities. Where the dark current results in an offset of the measurement and increases linearly with the scan time the error due to sensitivity variations increases linearly with the measured intensity. For scan times lower than 50ms as used for remote sensing from aircraft, the differenses of the dark current is small and thus negligible. The correction of the sensitivity variations results in a correction of each single sensor element. The correction coefficients have to be derived for each single CCD sensor. This can be done in the lab by measuring a homogeneously illuminated calibration surface or by averaging image data from a flight with sufficient data for statistical interpretation. It is assumed that the variations of the sensitivity are statistically independent and thus melt into a high-frequency signal. To remove other influences like that of the optical system

the correction coefficients are derived by high-pass filtering of the averaged sensitivity variations.

The optical system yields variations along the image lines. Vignette of the lens is dependent on the aperture and the lens itself. Additional filters result in further variations which are also dependent on the angle of measurement. Since the variations of the sensitivity are statistically independent along the sensor array they are different for the various spectral bands. The variations due to the optical system are a function of the pixel position, and thus the correction of one spectral band can be applied for each other band. This leads to the conclusion that it is always important to correct for the variations of the sensors but in case of the calculation of the NDVI with equation (4) it makes no sense to correct for the vignette.

Since measurements with the CLS are relative measurements the spectral channels only have to be calibrated to each other. To perform this a white source with equal radiation for all wavelengths from 400nm to 1000nm is necessary. A cheap and fairly good approach are thin clouds at the sky during midday.

The calibration of the CLS as an imaging NDVI sensor results into a calibration of the NDVI. This is carried out with an extension of equation (3) into

$$V_{NDVI} = S \; \frac{\gamma \left(I_{nir} - I_{nir,black}\right) - \left(I_{red} - I_{red,black}\right)}{\gamma \left(I_{nir} - I_{nir,black}\right) + \left(I_{red} - I_{red,black}\right)} \tag{4}$$

where $I_{nir,black}$ and $I_{red,black}$ are the offsets of the near infrared and red channels. The coefficient γ compensate for the different responses of the channels. It can be calculated with the numerator of equation (4) and the intensities of white radiation. The NDVI and with this the numerator has to be zero:

$$\gamma = \frac{I_{red,white} - I_{red,black}}{I_{nir,white} - I_{nir,black}} \tag{5}$$

This coefficient has to be derived from calibration measurements where $I_{red,white}$ and $I_{nir,white}$ represent the intensities of a white source. The channel offsets $I_{nir,black}$ and $I_{red,black}$ are measured with optically black sensor elements. Since these channel offsets are measured during the data acquisition only the calibration coefficient γ has to be calculated during the calibration measurements for the calibration of the NDVI data with equation (4).

6 GEO-CODING THE IMAGE DATA

The synchronization of the CLS to the data logger for the attitude and position data of the aircraft allows an attitude correction and geo-coding of the line scanner images. The data used for these corrections are recorded for each scanner line. The position of the aircraft is described as latitude A_{lat}, longitude A_{lon} and altitude A_{alt}, the attitude as pitch α_p, roll α_r and heading α_h angle.

The attitude correction and geo-coding are carried out in one step. The location on the ground for each pixel of the recorded image is calculated to be stored in any kind of a map image. Without any roll α_r or pitch α_p angle ($\alpha_r = 0$ and $\alpha_p = 0$) the centre element of the CLS will describe the track of the aircraft. They are pointing nadir. These pixel locations can be expressed by the position of the aircraft ($P_{lat} = A_{lat}$ and $P_{lon} = A_{lon}$). Real pitch and roll angles deviate from these positions.

Line scanners record whole image lines perpendicularly to the flight track. For each line the measurements are carried out with different viewing angles. Since these angles have the same orientation as

the roll angle their components could simply be expressed together:

$$\alpha_r^* = \alpha_r + \alpha_m \tag{6}$$

The angle of measurement of the line scanner α_m is dependent on the location of the pixel of the sensor array x_s, the size of the sensor as pixels $N = 2048$ and the spacing between the elements on the sensor array $s = 21\mu$m. For an optical scanner like the CLS the angle of measurement is

$$\alpha_m = \arctan \frac{s\left(\frac{N-1}{2} - x_s\right)}{f} \tag{7}$$

with f as focal length of the used lens and $(N-1)/2$ as the centre of the sensor array. x_s is counting from $x_s = 0$ to $x_s = N-1$ in N steps.

Each angle α_r^* and α_p implies a distance from the nadir, the track of the aircraft. These distances D_r and D_p can be calculated by the altitude of the aircraft:

$$\begin{aligned} D_r &= A_{alt} \tan \alpha_r^* \\ D_p &= A_{alt} \tan \alpha_p \end{aligned} \tag{8}$$

With the angle of heading α_h each of these distances can be separated into latitude and longitude parts:

$$\begin{aligned} D_{r,lat} &= -A_{alt} \tan \alpha_r^* \sin \alpha_h \\ D_{r,lon} &= A_{alt} \tan \alpha_r^* \cos \alpha_h \\ D_{p,lat} &= A_{alt} \tan \alpha_p \cos \alpha_h \\ D_{p,lon} &= A_{alt} \tan \alpha_p \sin \alpha_h \end{aligned} \tag{9}$$

The latitude and longitude parts can be calculated together and then be converted from metre to degrees. With the location of the aircraft the location on the ground for each pixel of the recorded image can be calculated:

$$\begin{aligned} P_{lat} &= A_{lat} + \frac{A_{alt}(-\tan \alpha_r^* \sin \alpha_h + \tan \alpha_p \cos \alpha_h)}{60 \cdot 1852\text{m}} \\ P_{lon} &= A_{lon} + \frac{A_{alt}(\tan \alpha_r^* \cos \alpha_h + \tan \alpha_p \sin \alpha_h)}{60 \cdot 1852\text{m} \cos A_{lat}} \end{aligned} \tag{10}$$

With these calculations it is assumed that a correct mounting of the CLS has been carried out with respect to the aircraft or position and attitude data are recorded for the line scanner itself. Since the GPS, the Inertial Navigational System (INS) or Vector GPS is permanently adapted to an aircraft and

the line scanner could be mounted and dismounted for the specific purpose each new mounting will result in a different orientation between these two systems. Beyond that, the position of the aircraft is not necessarily measured close to the line scanner system.

Eight parameters are important which can vary from one operation of the line scanner system to another. Not all parameters necessarily have to be determined for each measuring flight. Some are dependent on the aircraft used and some are fixed to a specific line scanner and lens. The eight parameters can be divided into three groups. The random errors change with each mounting of the line scanner to an aircraft. These are the errors in pitch δ_p, roll δ_r and heading δ_h angles in degrees. It is necessary to determine these parameters for each flight. Systematic errors are caused by the locations of the line scanner relative to the GPS antenna. D_x is the displacement perpendicularly to the fuselage centre line and counts positive if the line scanner is mounted on the right side of the GPS antenna. D_y is the displacement parallel to the fuselage centre line and counts positive if the line scanner is mounted in front of the GPS antenna. The vertical displacement has the same effect as the deviation of the ground elevation to the sea level. This is expressed in D_{ele}. D_x, D_y and D_{ele} are distances in metre. For the line scanner itself two parameters are critical for geo-coding of the images. The focal length f can vary from the specifications of the lens and thus have to be determined for each line scanner system. The eccentricity D_{ecc} indicates the displacement of the sensor line of the optical axis of the lens on the focal plane in pixels.

The last two parameters f and D_{ecc} extend equation (7) to

$$\alpha_m = \arctan \frac{s\left(\frac{N-1}{2} - (x_s - D_{ecc})\right)}{f} \tag{11}$$

The other six parameters are considered by means of the extension of equation (10):

$$\begin{aligned}
P_{lat} &= A_{lat} + \\
&\frac{(A_{alt} - D_{ele})\,(-\tan(\alpha_r^* - \delta_r)\ \sin(\alpha_h - \delta_h) + \tan(\alpha_p - \delta_p)\ \cos(\alpha_h - \delta_h))}{60 \cdot 1852\text{m}} - \\
&\frac{-D_x\ \sin(\alpha_h - \delta_h) + D_y\ \cos(\alpha_h - \delta_h)}{60 \cdot 1852\text{m}} \\
P_{lon} &= A_{lon} + \\
&\frac{(A_{alt} - D_{ele})\,(\tan(\alpha_r^* - \delta_r)\ \cos(\alpha_h - \delta_h) + \tan(\alpha_p - \delta_p)\ \sin(\alpha_h - \delta_h))}{60 \cdot 1852\text{m}\ \cos A_{lat}} - \\
&\frac{D_x\ \cos(\alpha_h - \delta_h) + D_y\ \sin(\alpha_h - \delta_h)}{60 \cdot 1852\text{m}\ \cos A_{lat}}
\end{aligned} \tag{12}$$

All parameters exept the displacements D_x and D_y and the elevation D_{ele} can be determined with a test flight over a known terrain. At least three marker positions are necessary for the determination of all mounting errors. The measurements have to take place in a way that the marker positions are distributed along the scanner lines. Two marker positions are sufficient if only the random errors δ_p, δ_r and δ_h of the mounting are unknown.

For a simple approach to determine the parameters of the mounting error in a successive correction, the parameters are divided into two groups. The errors in pitch δ_p and heading δ_h are causing a

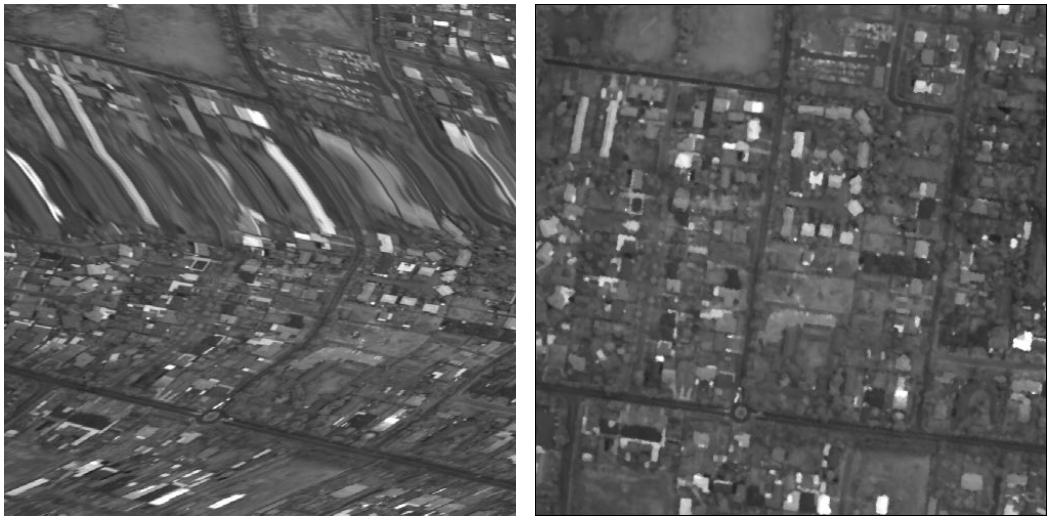

Figure 6: These images have been acquired near Parafield Airport in Adelaide, South Australia on 07.05.1999. The size of the images is 500m $\times$ 500m with a resolution of one metre. The images show the red band as a grey-level image. The left, image which appears distorted due to attitude variations, is geo-referenced into the right image.

displacement in flight direction. Once these errors have been corrected, the error in roll δ_r, the focal length f and the eccentricity D_{ecc} are only causing an error along the scanner line.

To demonstrate the process of geo-referencing, figure 6 shows two images which were acquired near Parafield Airport on 07.05.1999. The size of the images is 500m $\times$ 500m with a resolution of one metre. The images show the red band as a grey-level image. The left image, which appears distorted due to attitude variations, is geo-referenced into the right image.

7 RESULTS

Figure 7 shows the Parafield Airport area in Adelaide, South Australia on 07.05.1999. The size of the image is 3.3km $\times$ 1.8km with a resolution of one metre. The image is a mosaic of two overflights taken around solar noon. The survey was flown with the ARA Cessna 404 using a Honeywell^{TM} LaserNav INS to measure aircraft attitude at 50Hz and a 12-channel Novatel^{TM} GPS receiver for aircraft position and speed. The Novatel^{TM} GPS data is differentially corrected during post-processing using a GPS Base Station (another 12-channel Novatel^{TM} receiver). The flying altitude was 1300m above ground and the ground speed 50m/s. The bottom section of the image (approximately 1/3) was flown from right to left, the top section from left to right. The difficulty to identify the seam between the overflights illustrates the high accuracy of the automatic geo-referencing and mosaicing. The survey was carried out after many weeks without rain, indicated by the prevalence of the colours brown and yellow for an NDVI smaller than about 0.3. Only trees and shrubs (for instance, note the shrubs planted as a "PARAFIELD" pattern on the bottom side of the image) show higher vegetation indices, as well as some irrigated surfaces between the airport buildings.

The flight shown in figure 7 was also used to calibrate the installation of the CLS for mounting errors. For this purpose, several positions on the ground were accurately surveyed. Three of these points are necessary to determine the mounting error for this particular installation. After carrying out this calibration once, the geo-referencing process, as well as the mosaicing of individual overflights is carried out fully automatically, provided the scanner unit has not been removed from the aircraft.

As the survey area is rather flat (elevation variations no more than about 5m), there has been no correction for variations in elevation.

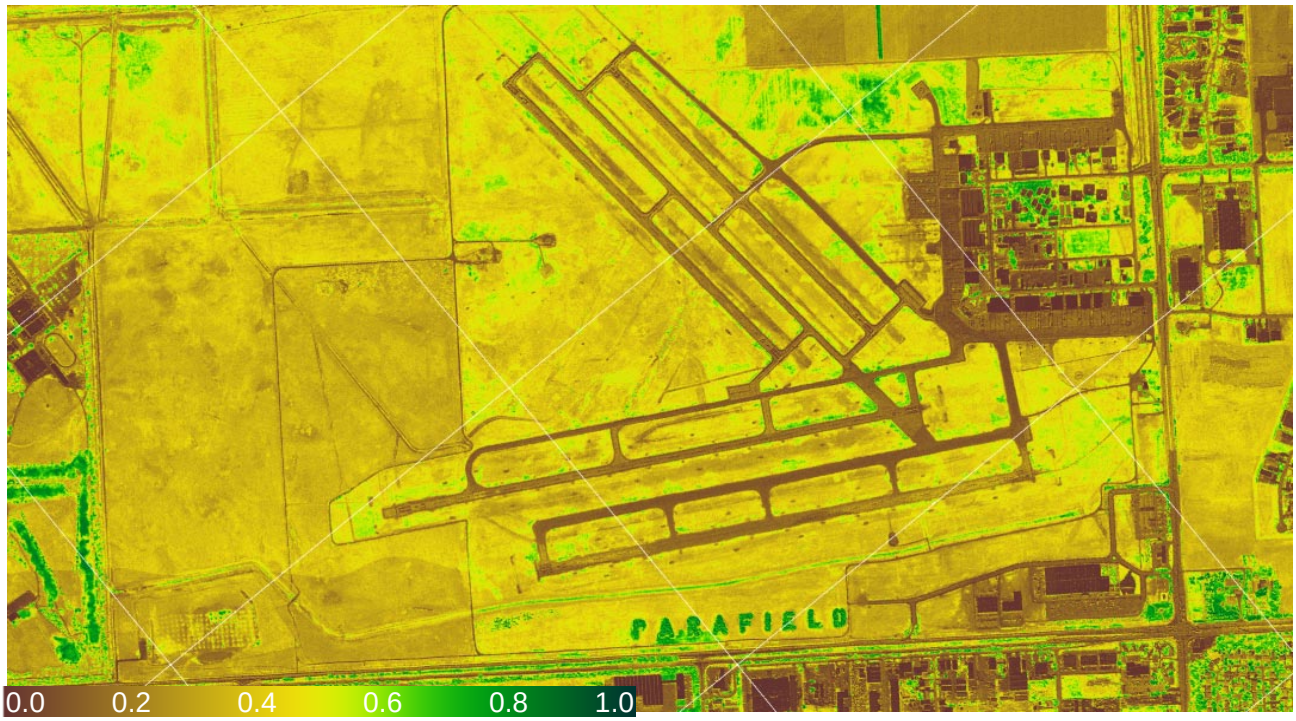

Figure 7: The image shows the Parafield Airport area in Adelaide, South Australia on 07.05.1999. The size of the images is 700m $\times$ 350m with a resolution of one metre. The NDVI ranges from $V_{NDVI} = 0.0$ to $V_{NDVI} = 1.0$ (see color scale).

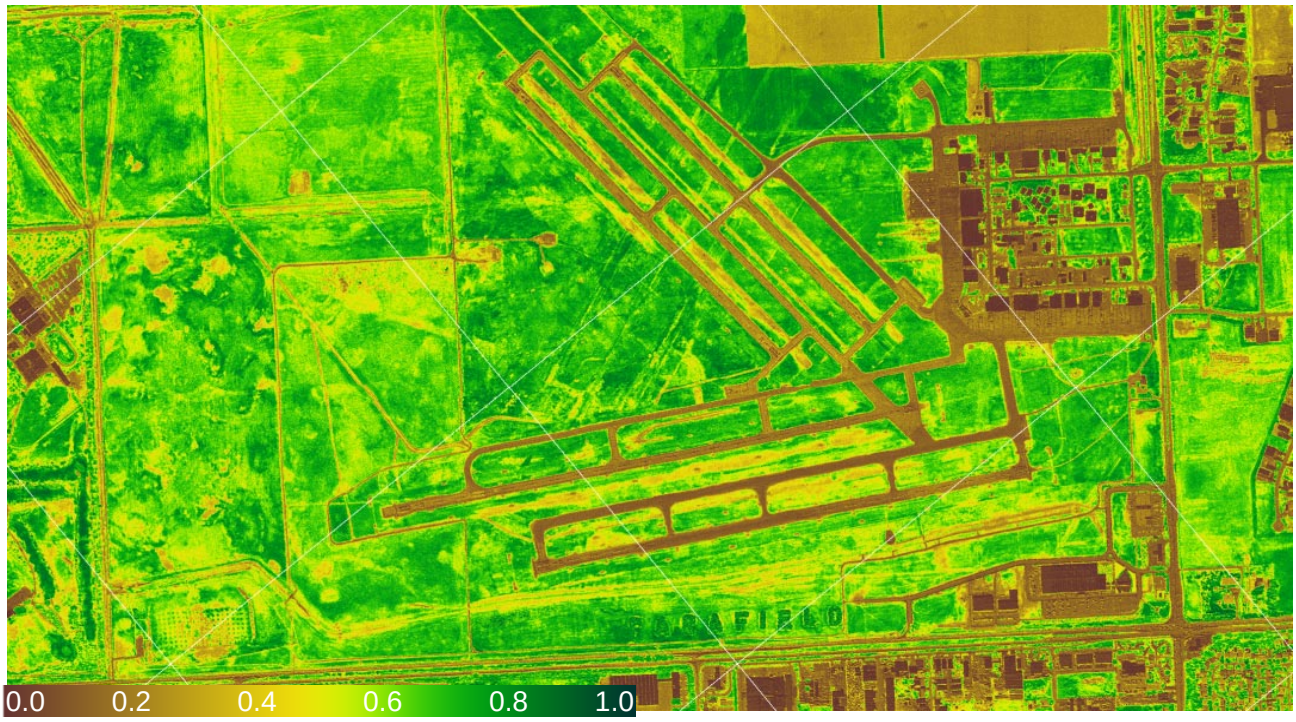

Figure 8: The image shows the same area as figure 7 on 26.07.1999. There has been more than 60mm rainfall during the previous two weeks. The NDVI image ranges from $V_{NDVI} = 0.0$ to $V_{NDVI} = 1.0$ (see color scale).

The same area was surveyed 19 days later on 26.07.1999 after more than 60mm of rain over the past two weeks and is shown in figure 8. All flight parameters were identical to the previous survey. The new vegetation growth caused by the rainfall is immediately visible. Several other features are also noticable, such as the enhanced visibility of old tracks, roads and runways caused by variations in vegetation density or amount, most probably related to differences in soil density and water availability.

Figure 9: These example images have been acquired at the Parafield Airport area in Adelaide, South Australia on 07.05.1999 (upper) and 26.05.1999 (middle). The size of the images is 700m $\times$ 350m. Between the two flights there had been over 60mm rainfall. These NDVI images range from $V_{NDVI} = 0.0$ to $V_{NDVI} = 1.0$. The difference image at the bottom shows the temporal variations of the vegetation. The difference ranges from $\Delta_{NDVI} = 0.0$ to $\Delta_{NDVI} = 0.5$ (see color scale). Black indicates areas of little change.

The two images of the top section of figure 9 show an enlarged section (700m x 350m) close to the images in figures 7 and 8, respectively, while the bottom image on figure 9 shows the difference between the two. On the difference image, the colour black indicates areas of little change, lighter colours indicate increasing NDVI from 07.05.1999 to 26.05.1999. The images show a cricket pitch and part of a golf course. Also noticeable is a water reservoir on the right side of the image which was only half filled before the rain and full afterwards. It is important to note that the difference image again was generated fully automatically without position adjustment.

Figure 10: The example images of irrigated vineyards were acquired near Langhorn Creek, South Australia on 19.02.1999. The size of the images is 1.3km $\times$ 1.0km with a resolution of 1.4 metres. The top image is generated with the green (500nm to 570nm) spectral band. The NDVI image at the bottom ranges from $V_{NDVI} = 0.2$ to $V_{NDVI} = 1.0$.

The example images of irrigated vineyards shown in figure 10 were acquired near Langhorn Creek, South Australia on 19.02.1999. The size of the images is 1.3km $\times$ 1.0km with a resolution of 1.4 metres. The top image is generated with the green (500nm to 570nm) spectral band. The NDVI image at the bottom ranges from $V_{NDVI} = 0.2$ to $V_{NDVI} = 1.0$. The comparison of these two images shows that cloud shadows will result in problems during the analysis of the image of the green spectral band. However, the NDVI image remains nearly unaffected even in conditions of patchy cloud shadows. Variations in the activity of the vegetation can only be seen in the NDVI image. The problem area below the dam was caused when levelling the field. Too much of the fertile soil had been removed in this region.

8 CONCLUSIONS

With the CLS and the associated processing software, a toolkit has been developed for rapid and very cost-efficient aerial surveys of land surface features for a wide range of applications. Prime products from the CLS are geo-referenced and mosaiced images of NDVI and false colour images at spatial resolutions as good as 0.5m. The high spatial resolution of 2048 pixels per scan line results in a high areal coverage. Due to the low weight and power requirements of the CLS, the package can be flown in low-cost aerial platforms. The availability of highly optimised processing tools and the non-requirement of interactive processing leads to a turn-around time between survey and end product of a few hours. Comparisons with other NDVI sensors lead to the result that the NDVI derived from measurements of the CLS is as reliable as the NDVI from the satellite sensors. These data could even be compared with each other.

ACKNOWLEDGEMENTS

The presented work was carried out while the first author was working under sponsorship of the Alexander von Humboldt Foundation, Germany, at Airborne Research Australia, the Major National Research Facility at the Flinders Univerity of South Australia.

REFERENCES

BANNEHR, L., 1990. Airborne Spectral Radiation Measurements in South Australia. PhD. Thesis. Flinders University of South Australia. 180 pp.

BOCHERT, A., 1992. Entwicklung eines Infrared-Line-Scanners für die Erdfernerkundung in Polargebieten und digitale Verarbeitung der erfaßten Signale. Alfred Wegener Institute, Bremerhaven, 575 pp.

BOCHERT, A.,1996. Klassifikation von Radarsatellitendaten zur Meereiserkennung mit Hilfe von Line-Scanner-Messungen. *Berichte zur Polarforschung*, **209,** Alfred Wegener Institute, Bremerhaven, 202 pp.

BOCHERT, A., 1999. Airborne Line Scanner Measurements for ERS-1 SAR Interpretation of Sea Ice. *International Journal of Remote Sensing*. **20,** 329–348.

BOCHERT, A. and WAMSER, CH., 1994. New Airborne Line Scanner Systems for High Resolution Sea Ice Observation. *The Global Atmosphere and Ocean System*, **2,** 247–251.

DATT, B., 1998. Remote Sensing of Leaf Chlorophyll Content in Eucalyptus Species.

DAWSON, T.P.; CURRAN, P.J. and PLUMMER, S.E., 1998. LIBERTY – Modelling the Effects of Leaf Biochemical Concentration on Reflectance Spectra. *Remote Sensing of Environment*, **65,** 50–59.

EIDEN, G.; DEISER, CH.; GESEL, G. and KÖNIG, T., 1991. Large Scale Monitoring of Rangeland Vegetation Using NOAA/11 AVHRR LAC Data. In: *Range Management Handbook of Kenya III/4*. Government of Kenya, Ministery of Livestock Development; Deutsche Gesellschaft für Technische Zusammenarbeit; Deutsche Forschungsanstalt für Luft- und Raumfahrt. Nairobi, Oberpfaffenhofen. 92 pp.

HARTMANN, J.; BOCHERT, A.; FREESE, D.; KOTTMEIER, CH.; NAGEL, D. and REUTER, A., 1996. Radiation and Eddy Flux Experiment 1995 (REFLEX III). *Berichte zur Polarforschung*, **218,** Alfred Wegener Institute, Bremerhaven, ??? pp.

HOPE, A.S.; PENCE, K.R. and STOW, D.A., 1999. Response of normalized difference vegetation index to varying cloud conditions in Arctic tundra environmants. *International Journal of Remote Sensing*, **20,** 207–212.

JUSTICE, C.O.; ECK, T.F.; TANRE, D. and HOLBEN, B.N., 1991. The Effect of Water Vapour on the Normalized Difference Vegetation Index derived for Sahelian Region from NOAA AVHRR Data. *International Journal of Remote Sensing*. **12,** 1165–1187.

KOTTMEIER, CH., 1993. User Handbook for the POLAR 2 and POLAR 4 research aircraft. Alfred Wegener Institute, Bremerhaven, 46 pp.

KOTTMEIER, CH; HARTMANN, J.; WAMSER, CH.; BOCHERT, A.; LÜPKES, CH.; FREESE, D. and COHRS, W., 1994. Radiation and Eddy Flux Experiment 1993 (REFLEX II). *Berichte zur Polarforschung*, **133,** Alfred Wegener Institute, Bremerhaven, 62 pp.

KRAMER, H.J., 1996. *Observation of the Earth and Its Environment.* (Berlin, Heidelberg: Springer), 1996

LEBLANC, S.G.; CHEN, J.M.; MILLER, J.R and FREEMANTLE, J., (1999). Compact Airborne Spectrographic Imager (CASI) used for mapping LAI of cropland. In *Proceedings of the Fourth International Airborne Remote Sensing Conference and Exhibition / 21th Canadian Symposium on Remote Sensing*, Ottawa, Ontario, I-297–I-303.

MCMICHAEL, C.E.; HOPE, A.S.; STOW, D.A.; FLEMING, J.B.; VOURLITIS, G. and OECHEL, W., (1999). Estimation CO_2 exchange at two sites in Arctic tundra ecosystems during the growing season using a spectral vegetation index. *International Journal of Remote Sensing*, **20,** 683–698.

PINAR, A. and CURRAN, P.J., 1985. Grass chlorophyll and the reflectance red edge. *International Journal of Remote Sensing*, **17,** 351–357.

SELLERS, P.J., 1985. Canopy reflectance, photosynthesis and transpiration. *International Journal of Remote Sensing*, **6,** 1335–1372.

WARDLEY, N.W., 1084. Vegetation index variability as a function of viewing geometry. *International Journal of Remote Sensing*, **5,** 861–870.